Voltage distribution in the windings of high temperature inverter-fed motors

Daniel Roger, Ewa Napieralska-Juszczak

Voltage distribution in the windings of high temperature inverter-fed motors

Abstract

Purpose − High temperature (HT^o) motors are made with inorganic coils wound with ceramic-coated wire. They must be carefully designed because the HT^o insulating materials have a lower breakdown voltages than the polymers used for insulating standard machines. The voltage distribution between coils during the repetitive transients caused by the fast fronted voltages imposed by the PWM inverter must be under a strict control.
Design/methodology/approach − The voltage distribution between stator coils is computed with high frequency equivalent circuits that consider the magnetic couplings and the stray capacitances. Two time-scales are used for getting a fast computation of very short voltage spikes. For the rst step, a medium time-scale analysis is performed considering a simplied equivalent circuit made without any stray capacitance but with the full PWM pattern and the magnetic couplings. For the second step, a more detailed high frequency (HF) equivalent circuit computes voltage spikes during short critical time-windows.
Findings − The computation made during the first step provides the critical time-windows and the initial values of the state variables to the second one. The rise and fall time of the electronic switches have a minor influence on the maximum voltage stress. Conversely the connection cable length and the common mode capacitances have a large influence.
Research limitation/implications − HF equivalent circuits cannot be used with random windings but only to formed coils that have a deterministic position of turns.
Practical implications − The proposed method can be used designing of HT^o machine windings fed by PWM inverter and for improving the coils of standard machine used in aircraft low pressure environments.
Originality/value − The influence of grounding system of the DC link is considered for computing the voltage spikes in the motor windings.

Keywords − PWM-fed motors. Ground connections influence. HT^o inorganic insulation. Distribution of voltage spikes.
Paper type − Research paper.

1 Introduction

The power density increase of electrical machines is a major challenge for many applications in aircrafts (Sarlioglu & Morris (2015), Sarlioglu (2014)). Physical limits derive from the rotor speed, the flux density in the air gap and the current density in the active conductors. The first and the second limits depend on mechanical and magnetic designs; the third one results on the overall thermal balance of the machine. The maximum temperature at the hottest point of windings is a major input data for the designer.

Today, the organic nature of standard electrical insulation system (EIS) is the major lock for operating at very high temperatures. The wide spread polymer EIS can be used up to 210^oC; the best ones can be used permanently up to 240^oC- 280^oC. Another solution is now opened with assessments on inorganic EISs, made without any polymer that can withstand permanently 500^oC (Iosif, Roger, Takorabet, Duchesne & Meibody-Tabar (2016)). Such EISs are made with ceramic-coated wires and HT^o cements instead of classical enameled wires and impregnating varnishes. With this technology, the HT^o machine windings are made of rigid inorganic coils placed on the stator teeth. This windings can be used for switched-reluctance synchronous motors (SRSM) or permanent-magnet synchronous machine (PMSM) when the rotor cooling is strong enough for getting a temperature compatible with the requirements of the best SmCo magnets (Rodewarld & Katter (2004)).

Today the HT^o motor winding technology is still at a low Technology Relevance Level (TRL 3 - proof of concept), developments are under progress. With this technology two perspectives are opened : electrical machines will be used in very hot environments such as the near vicinity of propulsion turbines of aircrafts; higher power densities will be brought by higher internal thermal gradients. However, the main drawback is the increase of the copper resistivity that makes higher Joule losses comparing to the classical machine designed for lower winding temperatures. When the maturity level of HT^o machines will be higher, they will stay in the narrow markets of specific applications.

The proposed development concern the design of motor-coils with a HT^o ceramic-coated HT^o wires that have poor insulation performances; the breakdown voltage is much lower than for the classical enameled wires (Iosif, Roger, Duchesne & Malec (2016*a*)). The turn-to-turn voltages must remain below 300V during the voltage

spikes due to fast-fronted voltage pulses imposed by the PWM inverter fed by the standard $540V$ High Voltage DC (HVDC) bus of more electric aircrafts. The paper proposes a detailed analysis of the voltage distribution of the voltage spikes in an inverter-fed HT^o PMSM. The study is performed in two steps with specific equivalent circuits; the transient states are computed with a SPICE simulator. First of all, an analysis for medium times is performed with a simplified equivalent circuit of the whole system, including the grounding connections, and the full PWM command. This first step gives data for another analysis that computes the short voltage spikes in critical time-windows. It uses a more accurate HF equivalent circuit of one phase of the machine and the fast-fronted pulses in the critical time-window defined in the first step. The method is applied to a 5kW PSMS HT^o prototype fed by a PWM inverter powered by the standard 540V bus of more electric aircrafts.

2 Principle of the simulation method

2.1 HT^o inverter-fed motor

Fig. 1 presents the concentrated windings of a 3-phase PMSM HT^o machine designed for compact applications. The rated frequency of this machine is 500Hz, it is made with 24 coils. The winding topology is classical for concentrated winding PMSM: the 8 coils of a phase are connected in series with a Y-coupling. The relative directions of the currents in the coils are designed for producing a 20-pole rotating field when the machine is fed by a 3-phase balanced sine supply produced by a standard PWM inverter (Pyrhonen et al. (2008)).

For high frequency phenomena following each fast fronted voltage edge of the PWM supply, the skin effects in the stator magnetic sheets is very strong, the magnetic field concentrates on the skin depth on each side or each magnetic sheet; there is no field in the in the major part of the sheet thicknesses (Roger et al. (2003)). However, the magnetic coupling between consecutive coils must be considered because the coils are very close to each other. Consequently, the whole stator circuit is modeled by 4 pairs of coils connected in series per phase (Roger, Toudji, Duchesne & Parent (2017)).

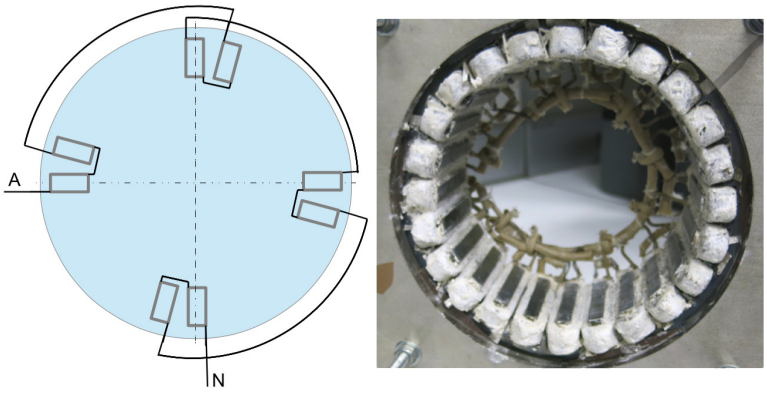

Figure 1: Phase A winding connections of a 24-20 PSMS and HT^o inorganic coils placed on stator teeth.

The machine is fed by a 3-phase PWM inverter able to control the machine. For safety reasons, the motor housing is connected to the grounding system. An electric connection exists also between the HVDC grounding system and the motor frame as shown in Fig. 2. The grounding system improve also the EMC performances of the whole drive. Fig. 2 shows also that each inverter leg is made of 4 electronic components (2 IGBTs and 2 diodes), which switches quickly a motor phase from the + to the - of the HVDC bus and conversely. Each inverter leg follows a Boolean command, which edges create a positive or negative fast voltage step in the whole circuit. Consequently, the whole circuit of Fig. 2 must be considered because the grounding connections have a capacitive coupling with the motor coils. With a non connected neutral point (N) of the motor, the common-mode capacitances have a major influence on the Neutral-to-Ground voltage and on the voltage stresses in windings.

Fig. 3 shows an example of a device that can be used for producing the HVDC bus with the associated grounding system. The power comes from the 3-phase AC source that can be the 50/60Hz grid or the 400-800Hz generator of an aircraft. The DC voltage is produced by a PD3 rectifier. For safety reasons, the source must be referenced to the ground or metal frame of the aircraft. The AC source is generally Y-connected; the neutral point (O) is connected to ground (G) by an impedance Z_N, which is often low. The phase inductances λ, used for studying the transients, are obtained by adding the AC source leakage inductances and the connection-cable ones. The resistances have a much lower influence, they can be neglected. The diodes sequentially connect the + and - outputs of the PD3 to the grid phases. Consequently, there is always an electric circuit between the HVDC + and - terminals and the grounding connections. The rectifier is generally followed by low-pass LC

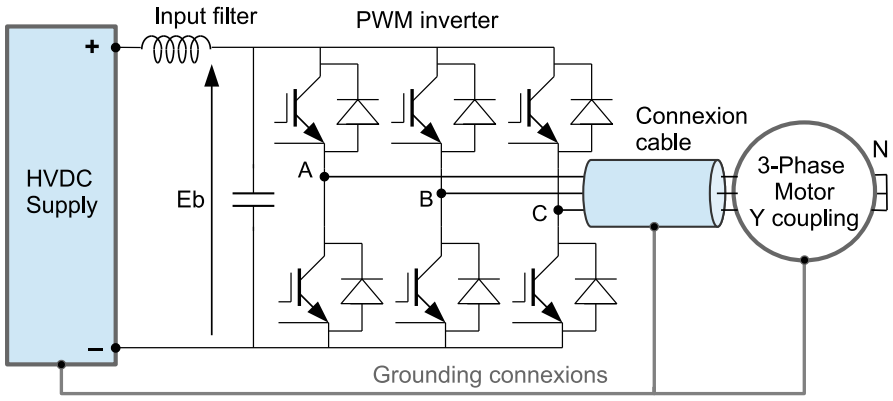

Figure 2: Inverter-fed motor with HVDC supply and grounding connections.

filters, placed at the input of each inverter fed by the HVDC grid, which limits the variations of the HVDC bus current. Therefore, the voltage drops in the line inductances λ remains small. The HVDC supply can be modeled by two DC sources with a middle point (O) connected to the ground (G) by the impedance Z_{OG}, which depends on Z_N. These equivalent circuit can also be used for the HVDC bus of aircrafts fed by more sophisticated rectifiers (Wheeler & Bozhko (2014), Prisse et al. (2009), Burgos et al. (2012)).

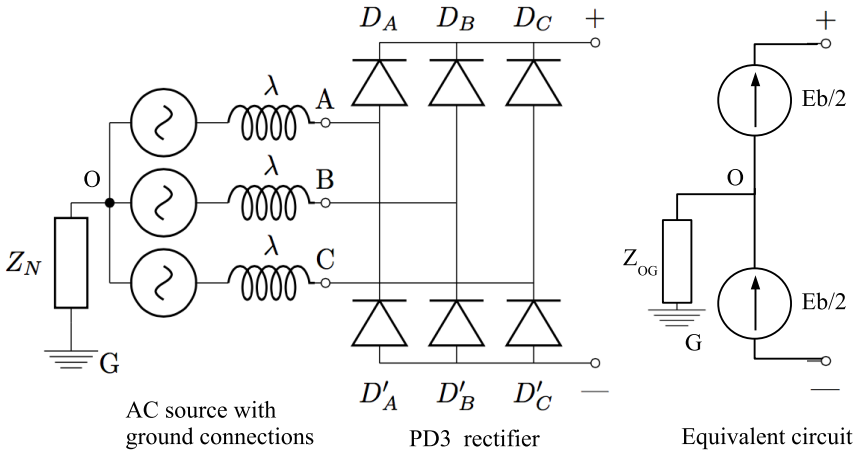

Figure 3: Example of a simple circuit for the HVDC supply.

A wide spread PWM command of inverter legs consists of using a triangular waveform corresponding to to the internal timer signal, which is compared to the sine reference for determining the Boolean commands. Fig. 4 is drawn for the phase A, it presents the res signal, the times one and the Boolean command x_A of the inverter leg A. The same timer signal is used for the phases B and C but the references are shifted by $2\pi/3$ and $4\pi/3$. The small circles in Fig. 4 are plotted at the ends of the edges of commands x_B and x_C built for the other phases. It can be seen that the probability to have a simultaneous switching of two phases is very low. Consequently, at the microsecond time-scale, the phases B and C can be supposed at steady state during the fast switching of the phase A. Fig. 4, the switching frequency is only 12 times higher than the motor low frequency for getting a good readability; the principle remains the same for higher switching frequencies.

2.2 Definition of the two time-scales of the analysis

The analysis of the voltage distribution in the motor windings must be made at a very short time scale because very short voltage spikes may cause an earlier ageing of turn-to-turn insulation leading to a local breakdown in windings (Lahoud et al. (2010)). Each fast-fronted voltage step causes complex transients in the whole circuit. Many inductances and capacitances are involved; the grounding connections have also an influence (Weidinger (2010)). The transients can be classified according to their natural frequencies. In the lower part of spectrum, only aperiodic transients are considered. They are due to the self and mutual inductances, the resistances and the PWM pulse patterns. In the upper part of the spectrum, the associations of inductances with stray capacitances must be considered because they yield high natural frequencies.

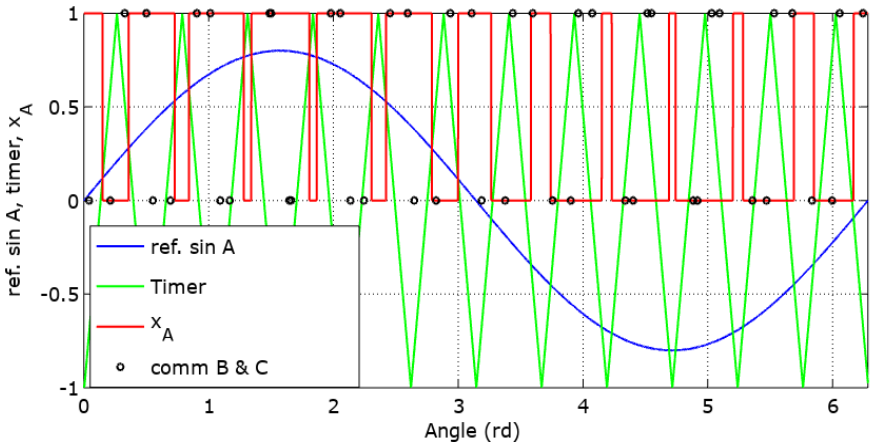

Figure 4: Typical command of the inverter leg A .

An equivalent circuit able to consider all these phenomena would be very complex and it should be computed for long times with a very small step time able to consider the highest natural frequencies. The proposed method works in two steps. The first step consists in analyzing the whole system at a medium time scale with a simplified equivalent circuit that considers only the low frequencies phenomena the simulation lasts several motor periods that correspond to many PWM periods. This analysis defines the critical time-windows for a motor phase. It also computes the initial charges of the common mode capacitances that influence he voltage spikes magnitudes defined for shorter times. The second step consists in computing the fast transients for only one motor phase with a more detailed equivalent circuit and a very short time step. This analysis is performed during the critical time-windows defined during the first step.

3 Simulations and results

3.1 Analysis for medium times

The mechanical transients corresponding to the machine control are not considered: the motor is supposed to be in a mechanical steady state. The first step of the analysis uses the simplified equivalent circuit of Fig. 5, which includes the ground connections (machine frame and connection inside the DC source). The neutral point of the motor (N) is not connected anywhere. The middle point of the DC bus (O) is connected to the ground by the impedance Z_OG depending on the DC bus safety technology. The three voltage sources are defined by the logical states of the inverter legs that depend on the PWM command. A simple RL circuit represents each coil. The common mode impedances are reduced to a high value resistance. This simplified equivalent circuit does not include any capacitance; the transients exited by the voltage step are aperiodic.

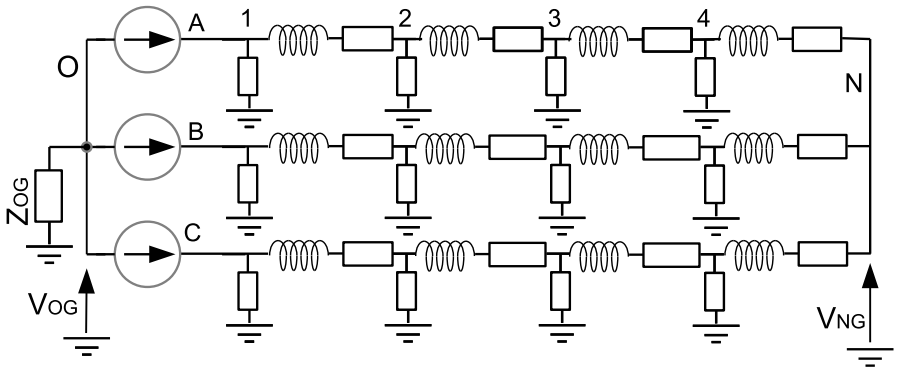

Figure 5: Equivalent circuit for a global study at a medium time-scale.

The simulation is made with a SPICE solver, which creates 3 voltage sources made of a large succession of segments defined by the PWM commands. The rise time and the fall time of the voltage pules does influence the medium time-scale equivalent circuit, they are set to a arbitrary value of $1\mu s$. A Matlab script automatically makes the file defining the SPICE circuit and the PWM command for the three phases. This equivalent circuit

is used for computing the phase currents and the voltages at the input and the output of each phase at any time The inverter legs impose voltage pulses between the phases and the HVDC middle point O. The phase-to-phase voltage is obtained calculating the differences between line voltages ($V_{AB} = V_{AO} - V_{BO}$, ...). the resulting currents are plotted in Fig. 7 for two motor periods. It can be seen that the steady state is obtained after the first period.

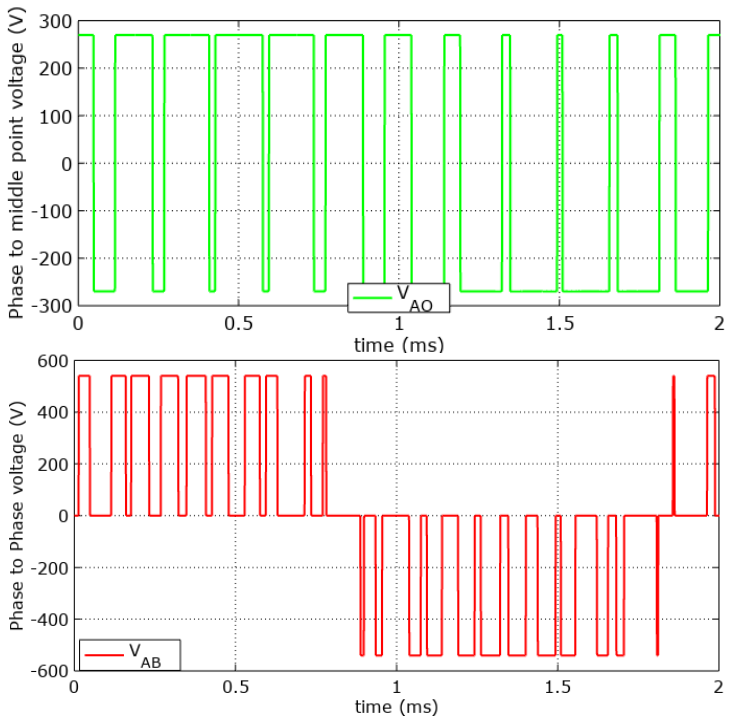

Figure 6: Voltages imposed by the PWM inverter for a full motor period.

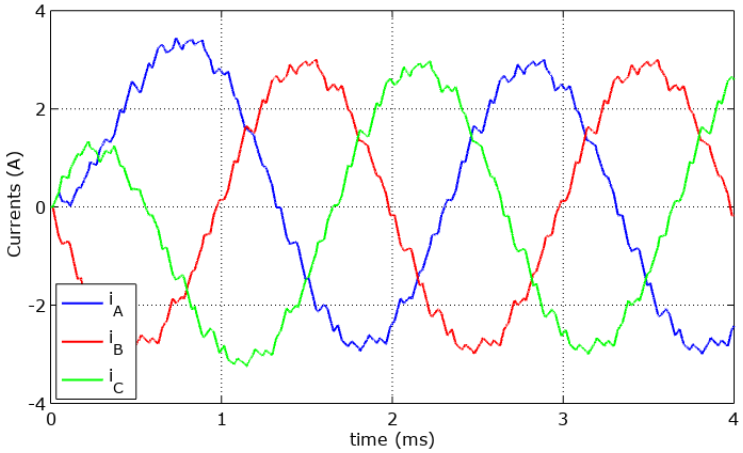

Figure 7: Line currents for 2 motor period.

With the standard Y-coupling, a phase of the machine does not see the phase-to-phase voltage because of the neutral potential (V_{NG}), which can be computed with the medium time-scale equivalent circuit of Fig. 5. Results are presented in Fig. 8 for a full low frequency period. The voltage between the neutral point and the ground is made of several pulses with 4 levels $\pm Eb/2$ ($270V$) and $\pm Eb/6$ ($90V$). The motor phases receive many pulses of various widths with 5 voltage levels: 0, $Eb/3$ ($180V$) and $\pm 2Eb/3$ ($360V$). The detailed analysis show that only a small number of voltage pulses applied to a phase of the motor corresponds to large voltage edges. One of them is emphasized in Fig. 8, it corresponds to a time-window between $t = 400\mu s$ and $t = 440\mu s$. This time-window is analyzed with another equivalent circuit that considers HF phenomena in windings.

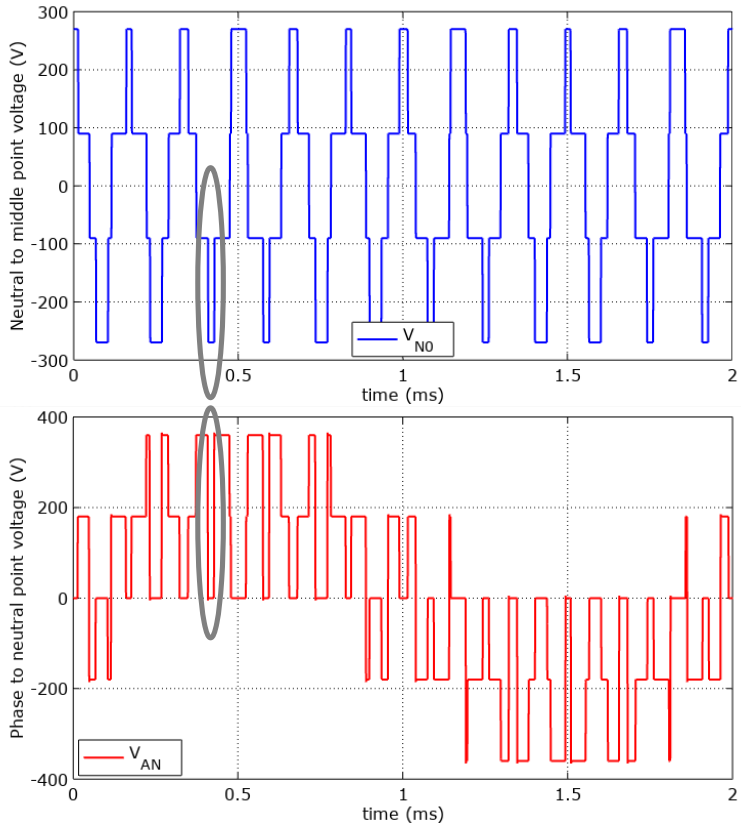

Figure 8: N-to-G voltage and Phase-to-Neutral voltage ($V_A - V_N$) for one motor period.

3.2 Analysis for short times

Fig. 9 is a zoom on the time-window defined above. It gives the voltage steps imposed at each end of the phase and the initial values that must be considered at the nodes 1, 2, 3 and 4 where the common mode capacitances of the HF equivalent circuit are connected. This figure shows also the two simultaneous voltage steps v_{AG} and v_{NG} imposed at both ends of the phase A. The negative edges are at $t = 408\mu s$ and the positive ones at $t = 427\mu s$. In Fig. 9, the slew rates are not representative of the switching times of the inverter that are much smaller, they corresponds to an an arbitrary value set to $1\mu s$ used for solving quickly the medium time-scale equivalent circuit of the whole machine and getting the initial charges of the common mode capacitances. For the short time-scale analysis, the actual switching times must be considered.

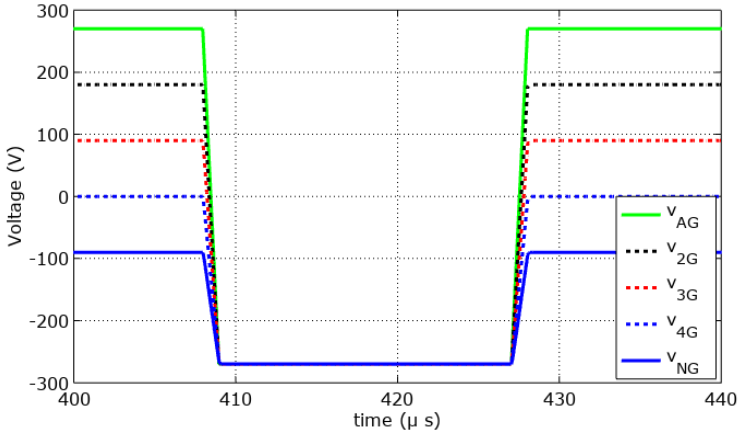

Figure 9: Voltages at both ends of the phase A ant at the equivalent circuit nodes for a critical time-window.

At the microsecond time-scale the transients can be studied with wave propagation theory (De Gersem et al. (2010)) or with detailed high frequency (HF) equivalent circuits. The second method has been chosen because

it is able consider the initial charges of the common-mode capacitances.

The connection cable is modeled by a T-cells per meter of cable. The RLC elements of the T-cells are obtained from classical HF measurements, in open circuit and in short circuits, performed on the cable with an impedance analyzer. The HF equivalent circuit of each coil pair is deduced from measurements performed with an impedance analyzer; The coil pairs are represented by the RLC equivalent circuit presented in the box of Fig. 10, which is able to take into account parallel and series resonance measured between $100kHz$ and $110MHz$ on a coil pair. The method for getting the model parameters is explained in Iosif et al. (2015). The common mode capacitances C_{M1} - C_{M4} and the parallel resistance are measured when the two coils of the pair are placed on the stator magnetic teeth.

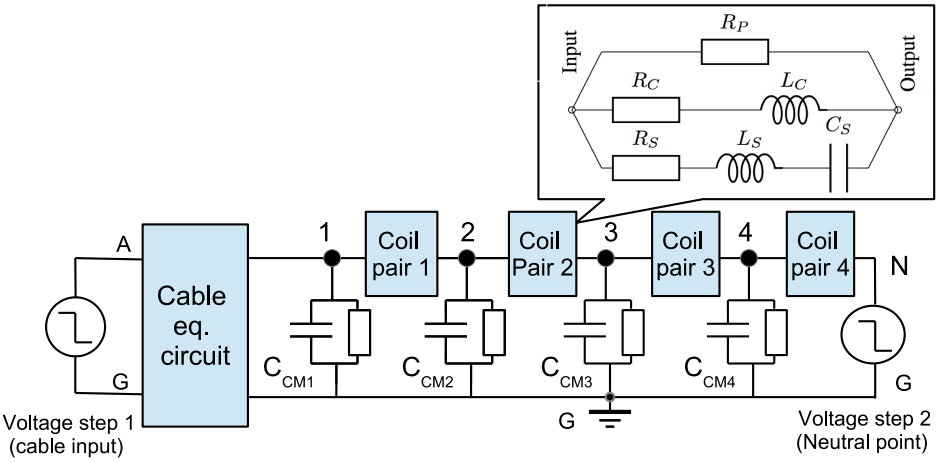

Figure 10: HF equivalent circuit of the phase A for the previously defined time-window.

The transient simulation is performed with rise and a fall times of $10ns$, which corresponds to recent SiC components. The time step of the SPICE solver is set to $1ns$. Results presented in Fig. 11 shows the voltages to the nodes of the HF equivalent circuit defined in Fig. 9 and the switching edges. The initial values at the internal nodes $1-4$ are computed with the medium time-scale equivalent circuit are considered. Results are presented for the first microseconds after the inverter switching because it corresponds to the largest voltage spikes. Two cable lengths ($1m$ and $10m$) are considered.The computation time is about 2 seconds on a standard laptop computer.

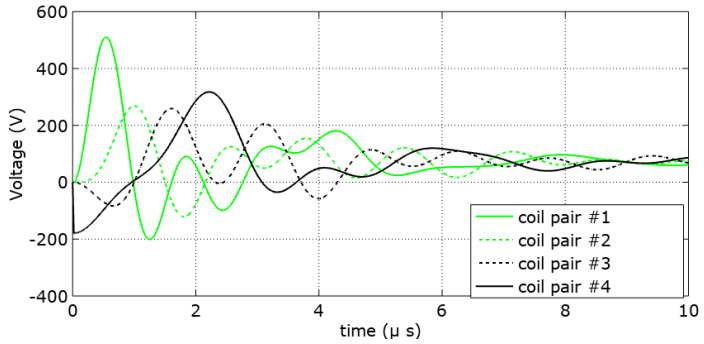

Figure 11: Voltages at the nodes for the first edges and two cable lengths.

The voltages steps v_{AG} v_{NG} have the initial and final values defined by the medium time analysis and with actual short switching times imposed by the electronic components ($10ns$). The curve v_{1G} shows the fast transient due to the connection cable. It lasts about $0.3\mu s$ for the short connection cable and more or less $3\mu s$ for the long one. For the long cable the propagation delay of $70ns$ is visible. These curves show also that the input voltage short spike, due to connection cable, in response to the negative input step is $-440V$ for the $1m$ length cable and $-660V$ for the $10m$ length one.

The transients states corresponding to the motor coil pairs are much slower (v_{2G}, v_{3G}, v_{4G}). Their magnitudes depends on the length of the connection cable; however this dependance is weak.

Figure 12 show the transient voltages between the terminals the first and the last coil pair of a motor phase; these voltages corresponds to the differences between the potentials at the corresponding nodes. The maximum

values correspond to the stresses that coils must withstand. It can be seen that maximum voltage applied to the first coil pair is higher that the maximum potential at the end of the feeding cable. This high value is due to the initial charges of the common mode capacitance C_{M2} which is positive pro a negative input spike.

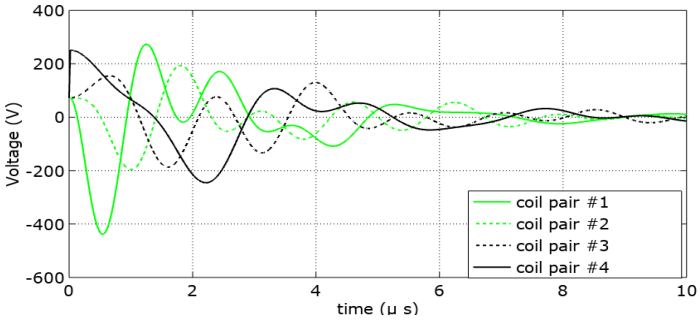

Figure 12: Voltages endured by first the the last coils for for the first edges and two cable lengths.

Figures 13 and 14 are similar but they are drawn for the positive edge. Results are similar but not identical with an opposite sign because the initial charges of the common mode capacitances are different.

The first coil pair must be designed for withstanding the highest voltage spike for the worst pulse configuration of the PWM. For 10-meter motor cable this stress is $720V$ and $660V$ for a very short cable of $1m$. These voltage stresses are much higher that the DC bus voltage ($540V$), despite the Y connection of the motor and the series connection of coil pairs within a phase.

This stress can easily be endured by a coil made of enameled wire designed for temperature under 240^oC and for atmospheric pressure. However, this voltage stress is too high for ceramic-coated wires able to withstand 500^oC, a specific coil design able to provide a good turn-to-turn voltage distribution inside coils is required (Iosif, Roger, Duchesne & Malec (2016*b*)). Similar specific designs must also be performed for motors used in the low pressure environment of aircrafts.

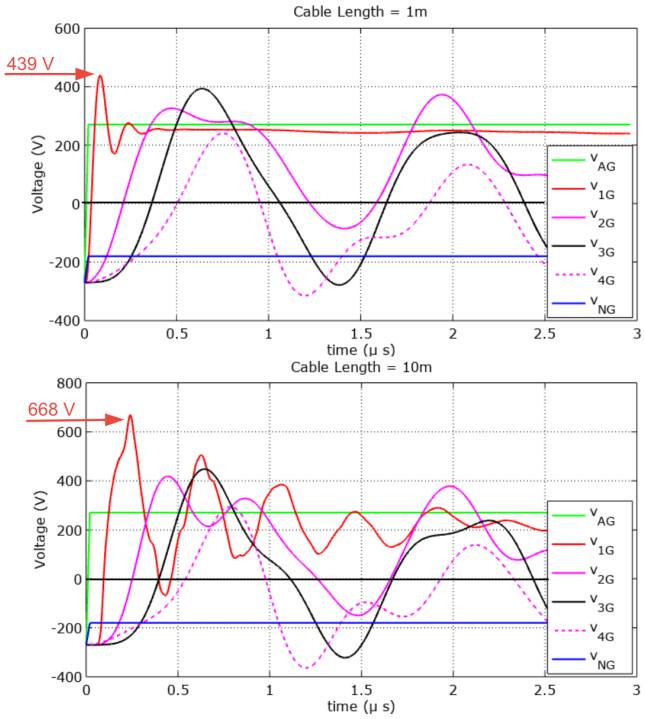

Figure 13: Voltages at the nodes for the second edges and two cable lengths.

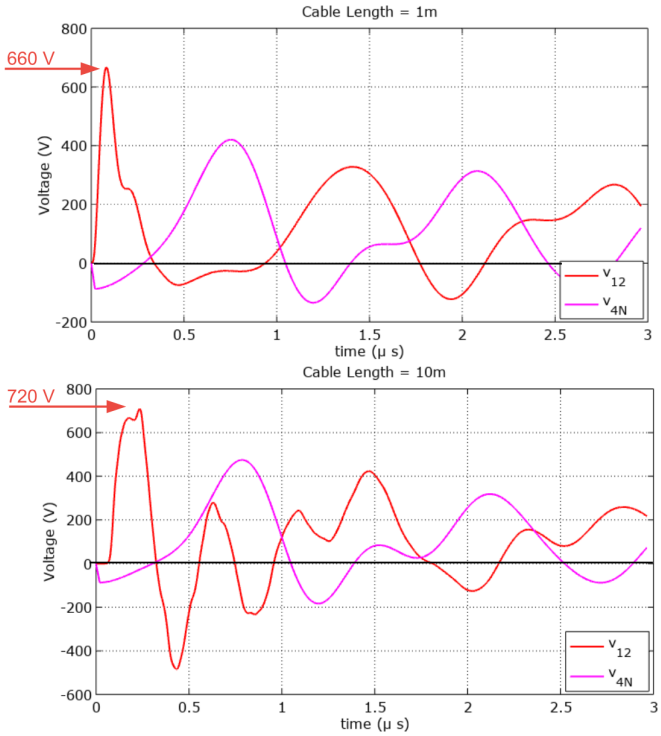

Figure 14: Voltages endured by first the the last coils or the second edges and two cable lengths.

4 Conclusion

The transient analysis performed for medium times with a simplified equivalent circuit and the full PWM pattern show that the grounding connections of the machine and of the DC supply of the inverter has a large influence on the voltage pulses received by a motor phase. This analysis shows also that the common mode capacitances existing between the coils and the motor frame connected to the ground influence the initial conditions of the transient state the produce the voltage spikes. This analysis shows also that, for a standard PWM method, the probability to have simultaneous switchings, at the microsecond time-scale, is very low. The transient corresponding to an inverter leg switching can be studied considering that the other phases are at steady state.

The proposed method, providing short computation times, is presented using a typical PWM command; it can also be used for other PWM technologies. The voltage distribution analysis was performed for designing a HT^o motor made with a ceramic coated wire that has poor electrical insulation properties. It can also be used for the design of long-life motors aimed at working in low-pressure harsh environment of aircrafts, which requires a very good distribution of voltage spikes between coils for avoiding PD. With such a fast simulation tool, it can be seen that he connection cable length and the common mode capacitances have a large influence on the maximum voltage stress endured by the first coil pair of each phase.

Previous measurements of the voltage distribution between the coils of the HT^o motor prototype where made with a standard 1-phase high slew-rate pulse generator. These experimental results shows a concentration of the electrical stress on the first coil (Roger, Iosif & Duchesne (2017)). This experimental study did not consider the initial charges of the common mode capacitances observed with the medium times analysis and the full PWM pattern. The previous measurements made with a single pulse under evaluates the actual electrical stress. A further experimental study is is planed with a PWM inverter feeding the 3 phases of the prototype. A specific design of the inverter command is under progress for providing the signals that are necessary for getting a correct synchronization of the fast oscilloscope on a narrow time window well defined.

References

Burgos, R., Chen, G., Wang, F., Boroyevich, D., Odendaal, W. G. & Wyk, J. D. V. (2012), 'Reliability-oriented design of three-phase power converters for aircraft applications', *IEEE Transactions on Aerospace and Electronic Systems* **48**(2), 1249–1263.

De Gersem, H., Henze, O., Weiland, T. & Binder, A. (2010), 'Simulation of wave propagation effects in machine windings', *COMPEL: The International Journal for Computation and Mathematics in Electrical and Electronic Engineering* **29**(1), 322–328.

Iosif, V., Duchesne, S. & Roger, D. (2015), Voltage stress predetermination for long-life designof windings for electric actuators in aircrafts, *in* 'IEEE - Annual Report Conference on Electrical Insulation and Dielectric Phenomena (CEIDP) - Ann Arbor', pp. 319–321.

Iosif, V., Roger, D., Duchesne, S. & Malec, D. (2016*a*), 'Assessment and improvements of inorganic insulation for high temperature low voltage motors', *IEEE Transactions on Dielectrics and Electrical Insulation* **23**(5), 2534–2542.

Iosif, V., Roger, D., Duchesne, S. & Malec, D. (2016*b*), An insulation solution for coils of high temperature motors (500 deg. c), *in* 'IEEE International Conference on Dielectrics (ICD)', Vol. 1, pp. 297–300.

Iosif, V., Roger, D., Takorabet, N., Duchesne, S. & Meibody-Tabar, F. (2016), Technological assessments for designing machines able to work at very high internal temperatures (450 - 500^{o}C), *in* 'Proceedings of the XXIIth International Conference on Electrical Machines Lausanne, Switzerland'.

Lahoud, N., Nguyen, M. Q., Maussion, P., Malec, D. & Mary, D. (2010), Using the design of experiments (doe) method to elaborate an electrical ageing model for the insulation of low voltage rotating machines fed by inverters, *in* 'Solid Dielectrics (ICSD), 2010 10th IEEE International Conference on', pp. 1–4.

Prisse, L., Ferer, D., Foch, H. & Lacoste, A. (2009), New power centre and power electronics sharing in aircraft, *in* '2009 13th European Conference on Power Electronics and Applications', pp. 1–9.

Pyrhonen, J., Jokien, T. & Hrabovcova, V. (2008), *Design of rotating electrical machines*, John Wiley & Sons.

Rodewarld, W. & Katter, O. (2004), Properties and applications of high performances magnets, *in* 'Vaccum-Schmeze GmbH'.

Roger, D., Iosif, V. & Duchesne, S. (2017), High temperature motors: Investigations on the voltage distribution in windings at a short scale times for a pwm supply, *in* '2017 IEEE International Electric Machines and Drives Conference (IEMDC)', pp. 1–7.

Roger, D., Ninet, O. & Duchesne, O. (2003), 'Wide frequency range characterization of rotating machine stator-core laminations', *The European Physical Journal – Applied Physics, EPJ-AP* **23**(2), 103 –109.

Roger, D., Toudji, M., Duchesne, S. & Parent, G. (2017), Concentrated winding machines fed by pwm inverters: insulation design helped by simulations based on equivalent circuits, *in* 'CEIDP'.

Sarlioglu, B. (2014), 'More electric aircraft - a reality', *IEEE Electrification Magazine* pp. 2–3.

Sarlioglu, B. & Morris, C. T. (2015), 'More electric aircraft: Review, challenges, and opportunities for commercial transport aircraft', *IEEE Transactions on Transportation Electrification* **1**(1), 54–64.

Weidinger, T. (2010), 'Common mode oscillations in electrical drive systems', *COMPEL - The international journal for computation and mathematics in electrical and electronic engineering* **29**(1), 221 – 234.

Wheeler, P. & Bozhko, S. (2014), 'The more electric aircraft: Technology and challenges.', *IEEE Electrification Magazine* **2**(4), 6–12.